ChemCatChem

Review
doi.org/10.1002/cctc.202301301

Chemistry Europe
European Chemical Societies Publishing

www.chemcatchem.org

VIP *Very Important Paper*

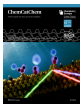

Exploring the influence of interfacial solvation on electrochemical CO_2 reduction using plasmon-enhanced vibrational sum frequency generation spectroscopy

Jaclyn A. Rebstock[+],[a] Quansong Zhu[+],[a] and L. Robert Baker*[a]

Although interfacial solvation plays an important role in determining carbon dioxide reduction (CO_2R) kinetics, present understanding of the potential dependent properties of the electrochemical double layer under conditions relevant for CO_2R remains limited. This article summarizes the development and recent applications of plasmon-enhanced vibrational sum frequency generation (VSFG) spectroscopy to study the effects of cation hydration and interfacial solvation on CO_2R using CO as a vibrational Stark reporter. Results show that electrolyte cations retain their entire solvation shell upon adsorption to inactive sites, while active sites retain only a single water layer between the gold surface and the cation. Measurements also show that the total interfacial electric field can be separated into two contributions: one from the electrochemical double layer (Stern field) and another from the polar solvation environment (Onsager field). Surprisingly, correlating VSFG spectra with reaction kinetics reveals that it is the solvation-mediated Onsager field that governs the chemical reactivity at the electrode/electrolyte interface. Measuring the interfacial water spectra during electrocatalysis also provides evidence for the proton source during H_2 evolution, which competes with CO_2R in aqueous electrolyte. These findings highlight the importance of directly probing cation hydration and interfacial solvation, which mediates reaction kinetics at electrochemical interfaces.

1. Introduction

Electrochemical CO_2R is an attractive approach to convert CO_2 to carbon fuels or other value-added products. Despite numerous studies of CO_2R on metal catalysts, a complete mechanistic understanding of this reaction is still lacking. For CO_2R to be commercially viable, improved control over the activity and product selectivity through design of the catalyst surface and/or electrolyte interface is needed. Classic electrochemical techniques with product detection allows mapping the activity and selectivity trends under a variety of conditions. However, from these techniques alone, the details of the electrochemical reaction mechanism at the electrode/electrolyte interface are insufficient to fully understand the properties that govern reaction activity and selectivity.

To gain better understanding of electrocatalytic reaction mechanisms, the use of operando spectroscopy has provided immense knowledge.[1] Optical, X-ray, and electron-based characterization techniques have all been used to better understand the catalyst structure and composition during CO_2R.[2–5] Vibrational spectroscopy has been of particular interest to measure surface adsorbed species, which can report information on the catalyst structure as well as the surface reaction mechanism. For example, carbon monoxide, CO, is commonly used as a vibrational reporter at electrode/electrolyte interfaces because it is a common intermediate of the CO_2R reaction on metals such as Au, Ag, and Cu.[6–10] Au electrodes in particular display high selectivity to CO. The Stark tuning behavior of adsorbed species such as CO (i.e., the rate at which the frequency shifts in response to the applied bias), is often used to study the magnitude of the electric field, which is related to the structure of the electrochemical double layer under CO_2R conditions.[9,11–13] The CO Stark tuning rate, electrochemical double layer structure, and CO_2R reaction rate are all influenced by the identity of the cation in the electrolyte solution with CO_2R reactivity following the trend: $Cs^+ \approx Rb^+ > K^+ > Na^+ > Li^+$.[14,15] Despite extensive research, the mechanism behind specific ion effects on CO_2R remains an open question. Certain models, such as Frumkin theory, attribute the reaction rate to the potential drop across the interface formed by the negatively charged electrode surface and the positively charged cation layer.[16,17] The magnitude of the interfacial electric field throughout the Stern layer of the formed electrochemical double layer is inversely proportional to the distance of hydrated cations from the negatively charged surface and depends on the size of the solvation shell around the cation. Consequently, some models consider that interfacial electric field plays an active role in mediating the reaction.[18–20] Other mechanisms have indicated that the cation-dependent pKa of hydrolysis determines reaction selectivity by controlling the interfacial pH during CO_2R.[14] Despite a number of open questions, it is clear that the cation-dependent properties of the electrochemical double layer play a critical role in catalytic activity and selectivity for CO_2R.

Additionally, CO_2R on metal electrodes is highly structure dependent, where undercoordinated step or edge sites on Au

[a] J. A. Rebstock,[+] Q. Zhu,[+] L. R. Baker
The Ohio State University
Columbus, OH 43210 (USA)
E-mail: baker.2364@osu.edu

[+] These authors contributed equally.

have drastically higher catalytic activity compared to terrace sites with higher coordination.[21–23] For polycrystalline Au electrodes, only a small fraction of the total available surface area is composed of undercoordinated sites responsible for the majority of the CO_2R turnover. Furthermore, CO adsorption on Au is weak, leading to low steady state surface coverage during catalysis.[21,23] This indicates that detection limits of a few percent of a monolayer are necessary to probe *in situ* produced CO at active sites on Au catalysts during active CO_2R.

Motivated by these important questions, this focused review summarizes the recent application of plasmon-enhanced vibrational sum frequency generation (VSFG) to study cation hydration and interfacial solvation on Au electrodes during active CO_2R using CO as a vibrational Stark reporter. As described below, this method enables detection limits of less than 1% of a surface monolayer during conditions of active CO_2R. Using this method we differentiate between CO adsorbed indiscriminately to the Au electrode due to CO purging of the electrolyte solution compared to intermediate CO formed selectively at active surface sites via *in situ* CO_2R. Accordingly, these studies provide important insights about cation hydration at active sites relevant for understanding the role of cation-mediated electric fields and interfacial solvation structures on CO_2R kinetics. Additionally, we show that measuring the interfacial water spectrum using VSFG provides insight into the various species present within the electrochemical double layer and the competition between possible proton donors for the H_2 evolution reaction, which competes with CO_2R in aqueous electrolyte.

2. *In situ* probing of electrocatalytic dynamics at solid/liquid interfaces with plasmon-enhanced VSFG

In situ detection of reactive intermediates during catalytic turnover can be a valuable tool to better understand complex reaction mechanisms; however, these measurements can be a challenge especially for catalytic reactions with a low steady state surface coverage such as CO_2R on Au. Plasmon-enhanced VSFG is compatible with *in situ* measurements of electrochemical interfaces and offers excellent detection limits, making it an ideal method to study specific cation effects during CO_2R on Au.[15,24–26] In the VSFG measurements that are discussed here, a narrow band 800 nm beam and a broadband mid-IR beam are combined at the interface to produce a VSFG signal beam that is the sum of the frequency of both input fields. In an electrochemical VSFG experiment, the beams can be coupled to the surface through either the electrolyte or through the electrode. Either method presents challenges: Coupling the beams through an aqueous electrolyte is difficult due to the intense IR absorption of water. This can be overcome by using an ultrathin layer of electrolyte sandwiched between a prism and the electrode surface, but this geometry introduces severe limitations on the transport of reactants and products to/from the electrode surface such that *in situ* measurements of catalytic processes occur under extreme mass transport limitations. Alternatively, coupling the beams through the electrode is challenging because most conductive electrodes are also not transparent. Use of ultrathin electrodes can increase transmission, but this leads to thermal instability of the electrode at high current density due to resistive heating. Consequently, despite the advantages of VSFG spectroscopy for studying electrochemical interfaces, studies of catalytic reactions at relevant current densities in the absence of mass transport limitations has remained difficult.

Jaclyn A. Rebstock received her B.S. degree in Chemistry from Minnesota State University in 2015 and then her M.S. degree from The College of William & Mary in 2020. Currently, she is a Chemistry Ph.D. candidate under L. Robert Baker at The Ohio State University. Her research focuses on studying the dynamics of heterogenous catalytic processes using vibrational sum frequency at metal and metal oxide interfaces.

Quansong Zhu received his B.S. degree in Environmental Engineering from Zhejiang University in 2019. He joined Prof. Baker's group in 2019, and is currently a Ph.D. candidate in Chemistry program. His research focuses on using ultrafast vibrational spectroscopy to study electrocatalytic interfacial process, such as CO_2 reduction.

L. Robert Baker received his B.S. degree from Brigham Young University in 2007 and his PhD from the University of California, Berkeley under the supervision of Gabor Somorjai. Following a postdoctoral fellowship with Stephen Leone, he joined The Ohio State University in 2014. His awards include the Coblentz Award in Molecular Spectroscopy, Emerging Leader in Atomic Spectroscopy, John von Neumann Distinguished Fulbright Fellow, Camille Dreyfus Teacher-Scholar Award, Young Innovator Award in Nano-Energy, and Journal of Physical Chemistry/PHYS Division Lectureship. He is the founding principal investigator of the NSF National eXtreme Ultrafast Science (NeXUS) facility. His research focuses on heterogenous electrocatalysis and developing spectroscopies to probe charge, spin, and solvent dynamics at catalytic interfaces.

To overcome these challenges in these studies, the beams are coupled to the electrode/electrolyte interface through an approximately 50 nm thick Au electrode. Although 50 nm Au is too thick to be transparent, efficient coupling of the electric fields is achieved through a surface plasmon resonance (SPR) in the Au electrode. This approach allows backside VSFG measurements on a stable electrode that can operate at current densities greater than 1 mA/cm^2 without any artificial mass transport limitations resulting from the *in situ* cell geometry. Figure 1a shows the set up of a plasmon-enhanced VSFG measurement for electrochemical measurements. The beams are focused to the Au/electrolyte interface through a CaF_2 hemicylindrical prism. The Au electrode is deposited on a CaF_2 window, which is index-matched to the prism using an IR transparent index-matching fluid to minimize beam attenuation as described previously.[24] Although phase matching into the SPR modes significantly enhances the VSFG signal, a disadvantage of using plasmonic catalysts is the large nonresonant background produced from the second-order response of the electrode, making it hard to detect vibrational resonances of species with low surface coverage. Rather than attempting to fit the convoluted resonant and nonresonant components and extract the resonance contribution, a time delay is introduced to the time asymmetric 800 nm beam relative to the IR beam, where the faster decoherence time of the nonresonant signal leads to nonresonant suppression and enhancement of the underlying resonance features.[27–29] To illustrate this, Figure 1b shows VSFG spectra convoluted with nonresonant background and C–H stretch modes from a self-assembled monolayer of dodecanethiol on Au before and after nonresonant suppression. With complete temporal overlap between the visible and IR fields, the spectrum is dominated by the nonresonant contribution. However, after applying an adequate time delay to the visible field and suppressing the nonresonant background, the C–H stretch modes of dodecanethiol become apparent.

Comparing the VSFG signal enhancement with calculations of the plasmon resonant Fresnel factors as a function of Au film thickness confirms the role of SPR to enhance the observed signals (see Figure 1c). Careful analysis of the angle and IR frequency dependence for this process shows that the momentum conservation requirements for SPR coupling are significantly relaxed due to the nanostructure of the Au film, which acts essentially as a grating with a broad distribution of line spacings.[26] We note here that a previous study from the Bonn group[30] has shown that the IR frequency-dependent Fresnel factor can influence the SFG spectra. The dispersion of

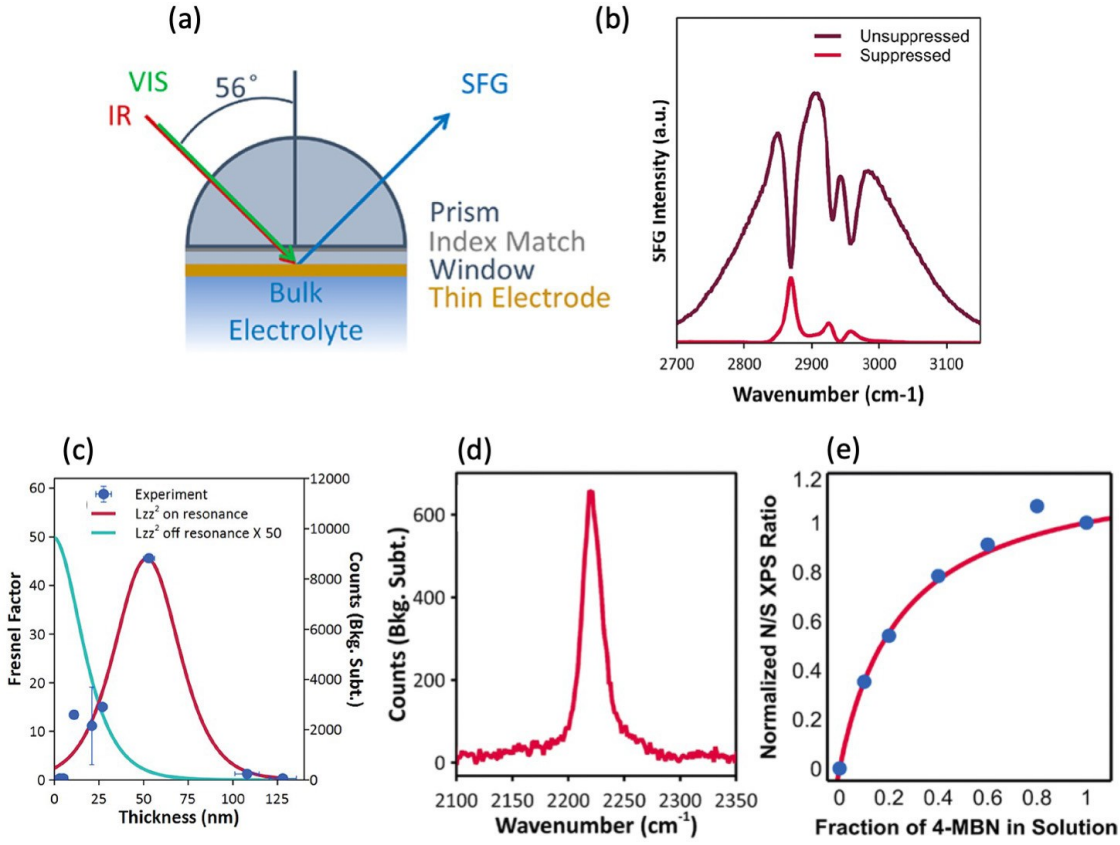

Figure 1. (a) Backside geometry of *in situ* VSFG measurements employed in this work. (b) Unsuppressed and nonresonant suppressed VSFG signal from a self-assembled monolayer of dodecanethiol at the Au/water interface. (c) Simulated on and off resonance Fresnel factor enhancement of the CaF_2/Au/water interface as a function of Au thickness. (d) Nonresonant suppressed VSFG spectra from 1% of a monolayer of 4-mercaptobenzonitrile coadsorbed with thiophenol at the Au/water interface. (e) Relative coverage obtained from the sulfur to nitrogen ratio collected from XPS as a function of 4-mercaptobenzontrile in solution. The line is a fit to the data using a competitive binding isotherm and was used to control the surface coverage. Adapted with permission from Ref. [24]. Copyright 2020 American Chemical Society.

the refractive index of the bulk water would lead to different enhancement to the interfacial electric field at specific IR frequencies, affecting the Fresnel factor and contributing to VSFG signal. For the VSFG spectra shown in the following context, a careful Fresnel factor calculation and correction have been conducted, which shows minor effect to the results. Consequently, although IR frequency-dependent Fresnel factors should be carefully considered in electrochemical VSFG studies, these considerations do not significantly influence the spectra presented and discussed here. The result is that the plasmon enhanced VSFG signal is relatively insensitive to IR frequency, incidence angle, and/or dielectric function of the electrolyte making this method highly versatile for probing electrode/electrolyte interfaces under a variety of relevant catalytic conditions.

Using the plasmon-enhanced VSFG method detailed above, very low detection limits can be achieved. The detection limit for this method was quantified by immersing Au electrodes in a solution of 4-mercaptobenzonitrile and thiophenol in a variety of concentration ratios.[24] The two species bind competitively with the Au surface, although only 4-mercaptobenzonitrile produces a vibrational signal at the CN resonance. After a mixed monolayer of the two species are formed on the Au surface, X-ray photoelectron spectroscopy (XPS) of the N 1s and S 2p edges were analyzed to determine the percent surface coverage of 4-mercaptobenzonitirle on the Au electrode (Figure 1e), and the results were fit using a competitive Langmuir isotherm model. Based on the determined equilibrium constants for the two adsorbates obtained from the Langmuir isotherm, Au electrodes were functionalized with control, and a 1% 4-mercaptobenzonitrile coverage was put on a Au electrode for VSFG measurements. Figure 1d shows the corresponding VSFG results of the CN stretch from the 1% monolayer coverage at the CaF_2/Au/water interface using a 670 fs time delay of the visible pulse (530 fs and 470 fs for the C–H and water region, respectively). This spectrum represents results of only a 60 s integration time, demonstrating the ability to readily detect surface adsorbates at low surface coverage consistent with the expected steady state surface coverage for CO on Au during CO_2R.

Figure 2a shows potential-dependent VSFG spectra within the CO stretch region in a CO_2-saturated 0.1 M $NaHCO_3$ electrolyte using plasmon-enhanced VSFG as a function of potential.[26] Starting from the bottom of the plot, 0.4 V vs SHE is applied to the Au electrode and then scanned cathodically to −1.5 V. Within this potential window, surface adsorbed CO from the CO_2R reaction is detected between 2116 and 2088 cm^{-1}, corresponding to an atop adsorption geometry. Figure 2b shows a cyclic voltamogram of the Au electrode over the same range of potentials confirming that these VSFG measurements

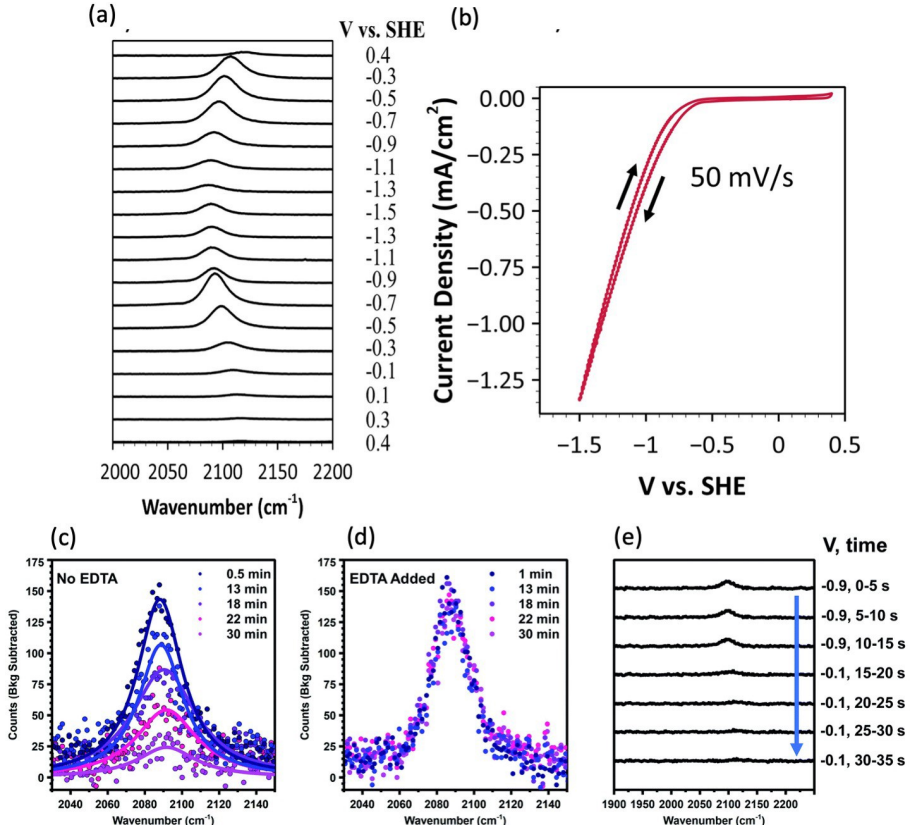

Figure 2. (a) *In situ* nonresonant suppressed spectra from atop CO during catalytic CO_2 conversion. (b) Typical cyclic voltammogram obtained during *in situ* measurements. (Reprinted with permission from Ref. [26]. Copyright 2020 American Chemical Society). VSFG spectra taken at −1.1 V vs Ag/AgCl in 0.1 M NaHCO 3 (c) without EDTA (d) and with 3 μM EDTA. (e) VSFG spectra taken at −0.9 V vs Ag/AgCl with 5 second integrations and then switched to −0.1 V vs Ag/AgCl. (Reprinted with permission from Ref. [25]. Copyright 2022 Royal Chemical Scociety.)

are obtained at catalytically relevant current densities. To confirm that the CO detected here is the result of catalytic turnover from CO_2 and represents an active surface intermediate, a number of controls were performed.[25,26] For example, prolonged CO_2R leads to poisoning of active Au surface sites by deposition of trace transition metal ion impurities.[31–33] Figure 2c shows the time-dependent CO signal during intentional deactivation of a Au catalyst in an impure electrolyte. Post-reaction XPS shows that complete deactivation occurs even when less than 4% of the total Au surface has been poisoned. Complete loss of the CO signal even when more than 95% of the Au surface remains accessible confirms that the CO detected here is formed by the *in situ* generation of CO from CO_2 at catalytic active sites, as compared to direct adsorption of solution phase CO, which would occur indiscriminately to the Au surface. Addition of the chelating agent, EDTA, prevents ion deposition,[31] and as shown in Figure 2d, this also preserves the CO signal intensity detected by *in situ* VSFG, showing a direct correlation between the VSFG signal and the time-dependent catalytic activity of the Au surface. Additionally, potential jump experiments, shown in Figure 2e, were performed where the CO species was detected under CO_2R electrolysis at -0.9 V vs Ag/AgCl, and then quickly switched to nonreduction conditions at -0.1 V vs Ag/AgCl where no CO is produced. The CO feature quickly disappears in less than 10 s, further confirming that the vibrational feature represents loosely bound CO at catalytic sites observed under steady state turnover. Below we show that using CO as a vibrational Stark reporter of active sites on Au, it is possible to gain important insights into the site-specific solvation of cations present in the electrochemical double layer.

3. Revealing site-specific cation solvation trends

The magnitude of the frequency shifts observed in Figure 2a can be used to give information on the strength of the interfacial electric field and the distance of the outer Helmholtz-plane (OHP) from the charged surface. The vibrational frequency of the adsorbed molecule is a function of potential and can be related to the interfacial electric field using the following equation:

$$\omega(\phi) = \omega_0 - \Delta\vec{\mu} \cdot \vec{F}(\phi)$$

where $\omega(\phi)$ is the potential-dependent frequency, ω_0 is the frequency at the potential of zero charge and determined experimentally with electrochemical impedence spectroscopy, $\Delta\vec{\mu}$ is the Stark tuning rate, or the dipole difference of the molecule in response to the applied field, and $\vec{F}(\phi)$ is the potential-dependent electric field. Therefore, if $\Delta\vec{\mu}$ can be determined theoretically or experimentally, the electric field under catalytic conditions can be calculated using *in situ* VSFG.

The magnitude of the electric field originates from the potential drop across the interface to the OHP. Therefore, $\vec{F}(\phi)$ can be further broken down to $\Delta\phi/\Delta d_{OHP}$, where the potential drop, $\Delta\phi$, which can be estimated under Gouy-Chapman-Stern (GCS) theory, can be used to determine the width of the interface to the OHP (Δd_{OHP}). Since Δd_{OHP} is determined by the cation's hydration shell, the local interfacial solvation structure during catalysis can be deduced through Stark tuning analysis of adsorbed intermediate species.

It is often assumed that solvation structure follows a bulk cation solvation model at the interface, regardless of the surface site identity.[34,35] CO_2R, as stated above, is highly dependent on site structure. DFT calculations have shown that electric fields are most intense (by orders of magnitude) at sites with high curvature.[36] Studies have also shown that undercoordinated sites have a 20-fold increase in catalytic activity compared to sites of higher coordination.[21] Since interfacial solvation structure and the magnitude of the electric field are closely related, it is reasonable to assume that solvation structure would be distinct at these sites just as the activity/selectivity are unique here too. The assumption of bulk solvation at the interface likely arises from the lack of a reliable probe of the undercoordinated active sites, which sparsely populate the polycrystalline surface. Since CO intermediate coverage is so low on Au electrodes, CO gas is often directly purged into the solution to saturate the surface with adsorbed CO that does not participate in the CO_2R reaction, but increases signal-to-noise.[35,37] The potential-dependent adsorption of this inactive CO species occurs more positive than the CO_2R onset potential on Au shown in Figure 2b, and therefore does not probe the interface under relevant catalytic conditions and is not selective to the sites of high CO_2R activity. Because CO probes used in this manner are not local probes of catalytic active sites on Au and the measurements are not under CO_2R conditions, it is difficult to reliably conclude information on the CO_2R catalytic mechanism.

With the motivation to understand site-specific solvation structure, two species of CO Stark probes were employed at the Au/electrolyte interface to report at different sites representing different catalytic activity.[25] When CO_2 gas is purged into a 0.1 M $RbHCO_3$ electrolyte and a cathodic sweep is applied over the CO_2R potential range, VSFG spectra show the appearance of adsorbed atop CO at 2090 cm^{-1} at the start of the CO_2R onset potential and continues to grow with increasing potential (Figure 3a). This CO species was identified as *in situ* CO, detected at undercoordinated active sites on the Au electrode during active conversion on the surface. The identity and location of this CO species is depicted in Figure 3c. Conversely, when both CO and CO_2 gas are purged into the system (Figure 3b), a second spectral feature appears before the CO_2R onset potential. This CO species appears at a lower frequency and can be attributed to an inactive surface adsorbed CO species, previously reported in surface probe measurements. The different potential-dependent behavior of the two peaks also reveals their distinct identity. The high-frequency CO feature appears very near the onset of CO_2R while the other CO

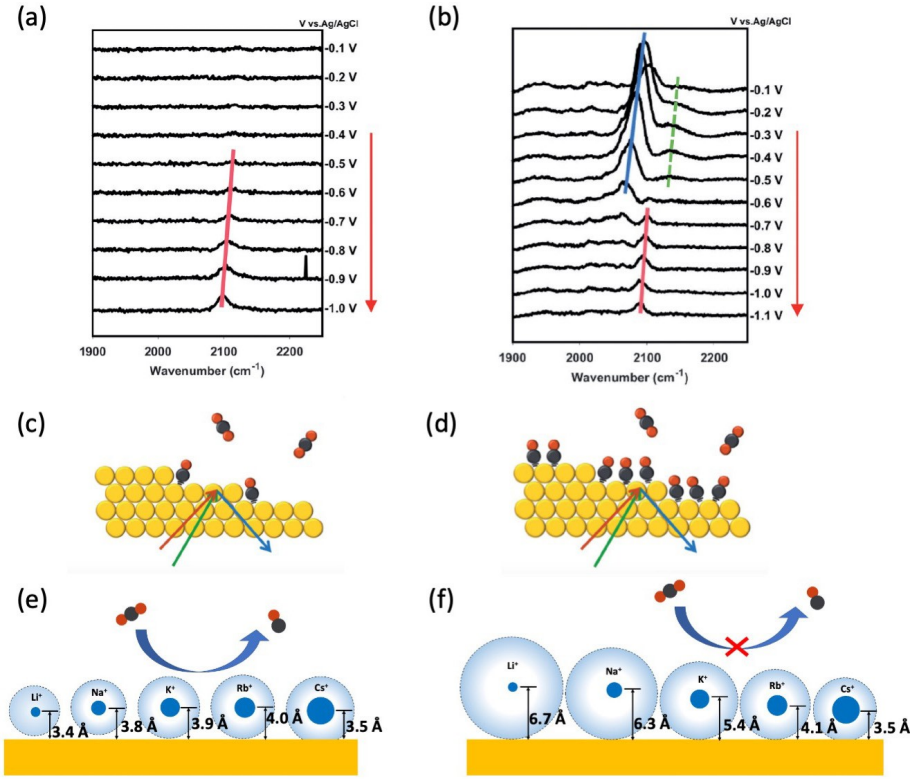

Figure 3. (a) VSFG spectra of CO_2-purged 0.1 M $RbHCO_3$ showing only *in situ* generated CO adsorbing to active sites. (b) VSFG spectra of CO_2 and continuous CO purging of 0.1 M $RbHCO_3$, showing both *in situ* generated CO adsorbing to active sites and purged CO adsorbing to spectator sites. (c) Diagram of CO_2-purged environment that results in CO at highly active undercoordinated sites (corresponding to Figure 3a). (d) Diagram of CO and CO_2-purged environment that results in CO at active undercoordinated and inactive terrace (spectator) sites (corresponding to Figure 3b). (e) Diagram of interfacial solvation structure at relatively inactive (terrace) sites. (b) Diagram of interfacial solvation structure at highly active (undercoordinated) sites. Adapted with permission from Ref. [25]. Copyright 2022 Royal Society of Chemistry.

species is observed only at potential positive of CO_2R, indicating the former is the active CO *in situ* generated at the Au surface, while the latter is inactive CO adsorbing at spectator sites. The poisoning experiment[25] confirms the active CO is generated from undercoordinated sites, and the inactive CO is adsorbing at terrace sites, consistent with previous reports.[38] Regarding the reason why active CO adsorbed at undercoordinated sites has a higher frequency, one possible explanation is that these undercoordinated sites behave more as single atoms with reduced electron density and therefore contribute less pi backbonding.[39] However, answering the question is beyond the scope of this work, and we hope future studies would provide more insight into this.

In addition to their absolute frequency positions, the two peaks differ in their potential-dependent adsorption behavior and Stark tuning behavior. Since the perceived frequency shifting of the CO species can be a convolution of Stark tuning as well as coverage dependent dipolar coupling, the possibility of dipolar coupling should be carefully investigated when using surface probes to measure interfacial electric field via the Stark effect. The coverage of the highly active sites on the Au surface is sparse, and therefore, there is little interaction between the CO reaction intermediates during steady state CO_2R at these sites.[26,40] For the higher coverage of inactive CO on the Au surface, dipole coupling effects were disentangled using previously reported methods,[41] and accounted for only 10% of the total shift in potential-dependent frequency. After accounting for CO coverage effects, the decoupled Stark tuning slopes can be compared between the two sites.

In order to obtain interfacial structural information from the frequency shifts and determine what solvation looks like at the two sites with different activity, the Stark tuning rate that describes the orientation and dipole difference of the infrared probe under an electric field, is determined through experimental calibration. Cs^+ is known to partially desolvate at charged catalytic interfaces, and has a reported OHP distance of 3.5 Å, determined from X-ray scattering measurements.[42] The VSFG data in 0.1 M $CsHCO_3$, is taken and the Stark tuning slopes are detected. Taking 3.5 Å as the absolute OHP distance for a Cs^+ electrolyte and estimating the potential drop over this distance using GCS theory, we obtain a calibration for the Stark turning rates of the CO adsorbed at the two different types of sites on a Au surface. For each CO species, a Stark tuning rate of 1.40 cm^{-1}/(MV/cm) and 4.29 cm^{-1}/(MV/cm) was determined for active sites and inactive sites, respectively. The units here refer to the frequency shift in response to the applied field. The Stark tuning rates for each CO species were used for all subsequent cation-dependent VSFG spectra. With the Stark tuning rates known, Δd_{OHP} is calculated for all cations and site specific solvation structure can be explored.

Based on the Stark tuning analysis presented here and calculated Δd_{OHP} values, Figure 3e,f provide a depiction of the cation-dependent solvation structure at the two sites. Here the distance from the Au surface to the OHP is taken as an approximation of the solvation radius of the adsorbed cation. At inactive sites (Figure 3f), cations follow a bulk solvation model where cations with smaller crystal radii, have larger hydration shells. The absolute value of these cation-dependent hydration radii almost exactly match the values obtained from bulk cation mobility measurements.[34] This result also matches previous spectroscopic analysis of the interfacial structure using a spectator CO molecule as an indiscriminate probe over the ensemble average of total surface sites. Surprisingly however, selective measurements at undercoordinated active sites that are responsible for the majority of the CO_2R on the Au surface show the complete opposite trend, where lighter cations such as Li^+ instead display a smaller distance from the Au surface to the OHP, that increases with increasing crystal radius (Figure 3e). Furthermore, the size of the solvation shell is drastically different between the two sites. While at inactive sites, the cations retain their entire bulk hydration shell, cations at active sites on Au shed the majority of the hydration shell only leaving one or, at most, two layers of water. These results highlight the following important conclusions related to cation-dependent CO_2R kinetics:

1) The identity of the surface probe is critical in obtaining accurate information about the CO_2R mechanism;
2) Solvation structure at the interface is complex and sites with different catalytic activity can possess different interfacial properties;
3) Efforts to understand electric field effects in CO_2R must rigorously account for site-dependent solvation structures since active and inactive surface sites on Au follow opposite trends in the cation-dependent electric field strengths as described further below.

4. Role of solvation-induced Onsager reaction fields during CO_2R

Considering the significant differences in the solvation structures between the active sites and inactive sites, as well as their distinct catalytic reactivity, it is important to understand the physical origin of this interesting correlation. Previous studies have recognized the solvatochromic shifts of vibrational reporters induced by solvents,[43–45] indicating the presence of electrostatic interactions, which can be further quantified by Onsager reaction fields.[46–48] This field is induced by the interaction of the solute dipole with the surrounding solvent and ions, where the solute dipole produces image dipoles in the surrounding medium. These solvent dipoles in turn sum to a net image dipole or "reaction field". Although this Onsager reaction field is primarily studied in bulk solutions, it may also exist at interfaces.[47] With the help of *in situ* VSFG measurements, we move forward to resolve the effect of this reaction field on catalytically active intermediates at interfaces during electrocatalysis, which may exceed the double layer electric field and have a dominant influence on the reaction.[15]

Denton et al. have performed careful measurements coupled with theory to understand the effect of water solvent molecules and cation solutes on carboxylate groups.[45] They observe the red shifts of the asymmetric stretch band of the C=O group when pairing with water molecules or Ca^{2+}. Interestingly, they find that the frequency shifts associated with solvation of the carboxylate group are almost exactly equal to the shifts induced by binding of the carboxylate group with a cation, indicating that the solvation-induced electric field is similar in magnitude to the field resulting from the ion pair. Additionally, Boxer and coworkers have discovered the solvatochromic shift of the nitrile and carbonyl group embedded in the solvent cavity in enzymes, which serve as the reporters of the extremely large electric field at active sites in enzymes as it enhances the catalytic reactivity.[49,50] Dawlaty and coworkers further extend the lesson learned about Onsager reaction field in bulk to the interface (Figure 4b,c), where the dielectric properties are inherently asymmetric.[47] However, a careful *in situ* study of the reaction field induced by solvation structures at the interface during electrocatalysis is lacking, which is important for designing a more efficient electrocatalytic system.

As described above, reaction intermediates can serve as local reporters from which we can derive the electric field within the Stern layer by analyzing the vibrational frequency shift.[9,13,51] However, the electric field generated by applied bias (Stern layer electric field, Figure 4a), and the Onsager reaction field generated by the net polarization of solvent molecules oriented by solutes (Figure 4b), are both present at the interface (Figure 4c). It is important to separate the contributions from each of them to understand the role of the solvation-induced Onsager reaction field. Recently we investigated the cation's effect on CO_2R, and successfully disentangled these two contributions to the total electric field.[15] Figure 4d–f give an example of how we estimate the individual contributions of these two fields. Here we note that the CO reporter is *in situ* generated from CO_2 reduction rather than spectator CO, as the feature is only observed after onset potentials. The black dots represent the potential-dependent frequency of these active CO intermediates obtained from VSFG measurement. They are extrapolated to the potential of zero charge (PZC) where the Stern layer electric field is minimized. Then the difference between CO frequency after onset potential and at PZC is used to calculate the Stern layer electric field (Figure 4a). The Onsager reaction field, on the other hand, is calculated from the difference of the CO frequency at PZC and under vacuum conditions, where there is no solvation (Figure 4b). The total field is the sum of both fields, and can be calculated from referencing the CO frequency under each potential to the frequency of CO adsorbed on Au in vacuum.

The strengths of the derived electric fields are shown in Figure 5a–c. No obvious trend is observed from the total field (Figure 5a) as a function of cations despite widely reported cation-dependent reactivity. However, once we disentangle the two fields, a cation-dependent trend becomes apparent. The strength of the Stern layer electric field decreases from Li^+ to

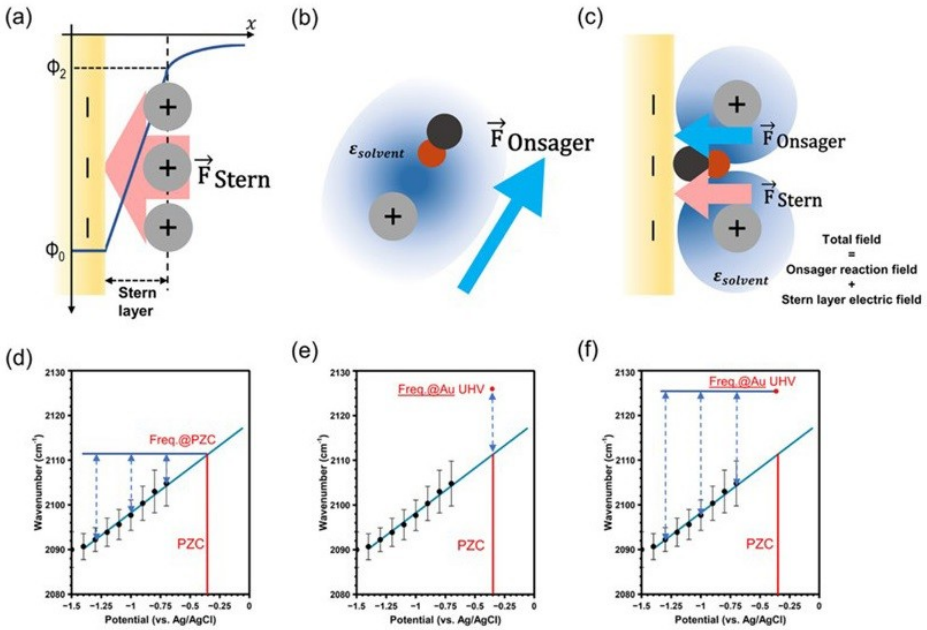

Figure 4. Diagram of (a) the Stern layer electric field at the electrode surface; (b) The Onsager reaction field in bulk solution (the black circle represents the carbon atom, and the red circle represents the oxygen atom); (c) The total field at the electrode surface, with contributions from both fields. Calculation of (d) the Stern layer electric field; (e) The Onsager reaction field; (f) The total field. Reprinted with permission from Ref. [15]. Copyright 2022 American Chemical Society.

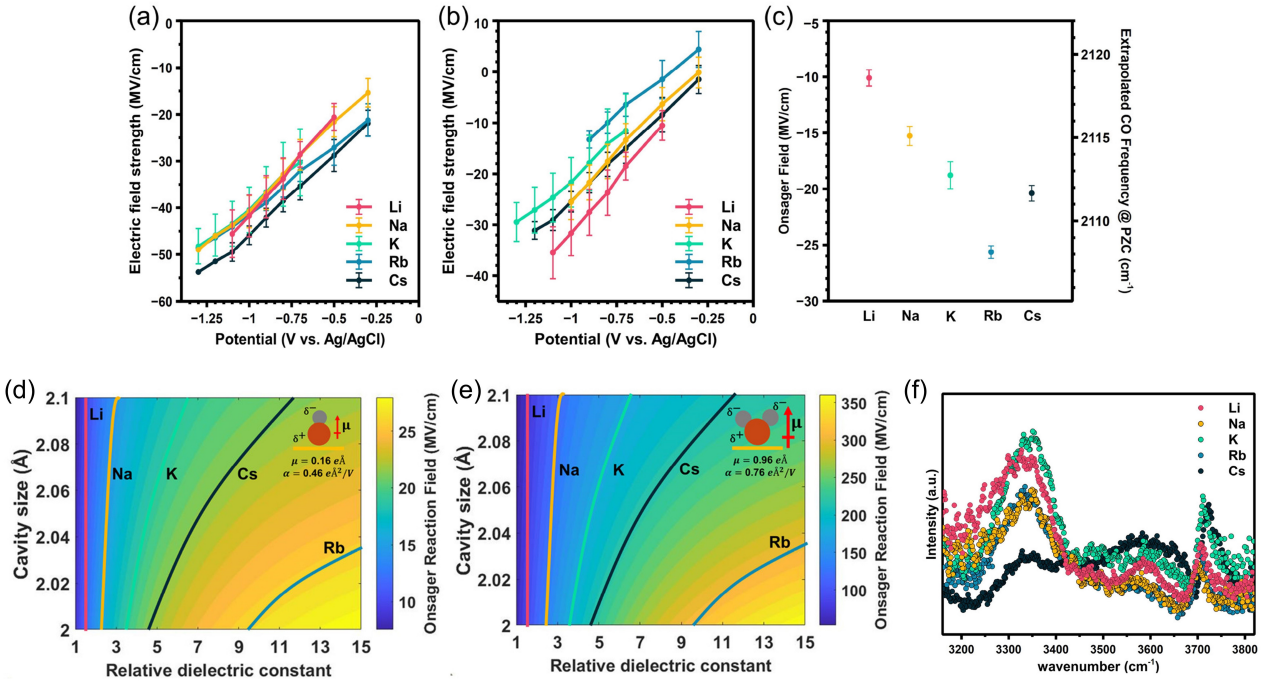

Figure 5. The derived potential-dependent (a) total field strength; (b) Stern layer electric field strength; (c) Onsager reaction field strength. The derived Onsager reaction field as a function of the cavity size and relative dielectric constant for (d) the adsorbed CO; (e) the adsorbed bent CO_2. (f) water spectra in different cation solutions measured with VSFG. Adapted with permission from Ref. [15]. Copyright 2022 American Chemical Society.

Rb^+, and increases at Cs^+ (Figure 5b), which is a direct result of their different solvation radius, as discussed in the previous section. In contrast, the Onsager reaction field shows the opposite trend (Figure 5c). Importantly, the Onsager reaction field and not the double layer field shows a strong correlation with the cation-dependent CO yield, suggesting that the solvation-induced Onsager reaction field is important for determining the reaction kinetics.[15]

Considering that the rate of CO_2 activation may depend on the field,[19,36,52,53] it is important to consider why reactivity shows a strong correlation with the Onsager reaction field as compared to the Stern layer contribution, which has similar magnitude. To understand this, we employ the equation of the Onsager reaction field at the interface as derived by Dawlaty and coworkers,[47] to derive the cavity size and relative dielectric constant (Figure 5d) from Figure 5c. Then we calculate the Onsager reaction field imposed on the key intermediate, CO_2^-, involved in the rate determining step (RDS) of CO_2R, since it has a significantly greater dipole moment compared to CO. Surprisingly, the Onsager reaction field felt by CO_2^- is predicted to be on the scale of hundreds of MV/cm (Figure 5e), an order of magnitude stronger than the Stern layer electric field (Figure 5b). This may explain why the CO_2R catalytic performance is correlated with the Onsager reaction field rather than the Stern layer electric field, assuming that the cation-dependent interfacial solvation structure is primarily responsible for stabilizing the rate determining transition state during electrochemical activation of CO_2.

This work has provided mechanistic insights into how solvation structure is affecting the electrocatalytic CO_2R through the RDS. However, the solvation structure has been derived from the CO spectra, which is an indirect reporter. The direct monitoring of water structure with VSFG would provide more accurate information. The preliminary water spectrum in different cation solutions has shown an interesting trend regarding the water feature at around 3350 cm^{-1}, which stays similar for Li^+ to Rb^+, but decreases significantly at Cs^+ (Figure 5f). It is likely that this observation correlates with the partial desolvation of Cs^+ as discussed in the previous section. However, the physical assignment for this feature is not clear. To gain deeper insights into the interfacial solvation structure under conditions relevant for CO_2R and the hydrogen evolution reaction (HER), we have initiated a systematic investigation by directly probing the vibrational spectrum of interfacial water molecules using VSFG.

5. Interpreting solvation-affected catalysis through directly probing interfacial water

Although there have been many studies about interfacial water structure at solid-liquid,[54–58] liquid-liquid,[59,60] and air-liquid[61–65] interfaces, as probed by VSFG, most of them are *ex situ* measurements without applied bias. Tong et al. has successfully observed the *in situ* generated free-OH feature from water reorientation as a response to the applied bias at a Au surface using VSFG,[66] and Rehl et al. has discovered that water molecules in the Stern layer and diffuse layer respond differently to the silica surface potential change.[57] However, neither of these studies are conducted under conditions of active catalytic turnover. Recently we succeeded to observe an *in situ* generated hydroxide feature from HER during CO_2R.[67] The qualitative interpretation of this OH^- feature in combination with other bands in the interfacial water spectrum has provided important insights toward understanding the influence of electrolyte composition and solvation effect on CO_2R and HER.

We first show the results from probing the Au surface in Ar-purged Na_2SO_4 solution, and two features are clearly observed (Figure 6a). The feature at around 3730 cm^{-1}, which appears before the onset potential of HER, can be assigned to free-OH due to the hydrophobic nature of Au.[61,62,66,68]

The other feature at around 3650 cm^{-1}, however, only appears after the onset potential and grows at more negative-potentials. After performing careful control experiments, we assign it to the *in situ* generated OH^- anion from HER. To our

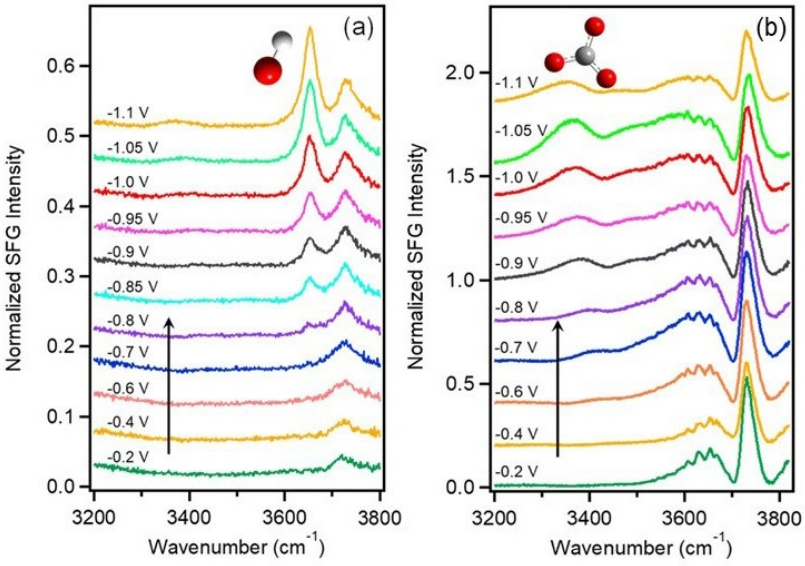

Figure 6. Potential-dependent VSFG spectra of water obtained from 0.05 M Na_2SO_4 solution purged with (a) Ar; (b) CO_2. Adapted with permission from Ref. [67]. Copyright 2023 The Royal Society of Chemistry.

best knowledge, this is the first direct observation of hydroxide produced inside the Stern layer. We also present comparative spectra obtained while purging CO_2 into the Na_2SO_4 solution. Interestingly, the OH^- feature disappears and another broad feature appears at around 3350 cm^{-1}, similar to the one we observed in Figure 5f. Based on pH-dependent control experiments, we assign this band as a carbonate feature likely originating from the hydrogen bonded water molecules surrounding CO_3^{2-} (HCO_3^-) anions. The disappearance of the OH^- peak is correlated with the switching of the proton donor during potential-dependent HER, as discussed below. It is estimated that at the electrolyte concentrations used here the vibrational dephasing time of interfacial water is on the order of 700 fs.[69] Considering the measurement is taken with a 467 fs delay of the visible beam relative to the IR, we selectively suppress the nonresonant response from the Au electrode while maintaining high sensitivity to interfacial water.[67] Importantly, this time delay of 467 fs is also substantially longer than the bulk water dephasing lifetime of 200 fs. Due to the presence of a DC field at the electrode/electrolyte interface under applied potential the VSFG spectra may include a significant contribution from the $\chi^{(3)}$ response of bulk water, which undermines the desired interfacial sensitivity. However, the 467 fs time delay is sufficient to mostly suppress this $\chi^{(3)}$ response. Here we note that we have carefully quantified the $\chi^{(3)}$ bulk contribution to the water spectra shown here, and it was determined to be less than 20% due to the time delay between IR and visible beams.[67] Thus the contribution from $\chi^{(3)}$ in these reported spectra is small.

Figure 7a shows the water spectra obtained from a Au surface in 0.1 M $NaHCO_3$ solution purged with Ar. The OH^- feature appears after the onset potential and continues increasing, while the carbonate feature increases first and then decreases at more negative potentials. The potential-dependent intensity change for these two features is plotted in Figure 7b, which clearly shows two regions. Before −1.0 V, the CO_3^{2-} feature increases rapidly but the OH^- feature remains stable, while at potentials below −1.0 V, the OH^- feature grows rapidly while the CO_3^{2-} feature begins to decrease. This change in the intensity trend is explained by the switching of proton donors as a function of potential. Above −1.0 V, HCO_3^- (H_2CO_3) is likely to be the proton donor which directly produces CO_3^{2-} rather than OH^-. However, below −1.0 V, water becomes the proton donor and directly generates OH^-. The accumulation of cations within the double layer at more negative potentials would exclude water molecules and disrupt the H-bonding network,[70,71] which could help explain why the carbonate feature slightly decreases even if the carbonate anion concentration may increase when the HCO_3^- buffers with OH^-.[67]

Although this finding is focused specifically on HER kinetics, it demonstrates that water molecules outcompete bicarbonate as the proton donor within the double layer in the relative potential region for CO_2R. Bicarbonate anions could provide protons for CO_2R in less negative potential regions, considering its lower pKa (10.32 for HCO_3^-, and 6.37 for H_2CO_3) and potential ion-pairing with the cation.[72,73] However, water molecules would probably replace them as the proton donor for CO_2R in more negative potential regions as the interfacial anions are repelled from the electrode by the enhanced electric field.

This study highlights the importance of solvation structure at the interface since it could not only template the local electric field, but also participate in the kinetic competition between HER and CO_2R. *In situ* electrochemical VSFG is uniquely suited to these studies compared to other spectroscopic

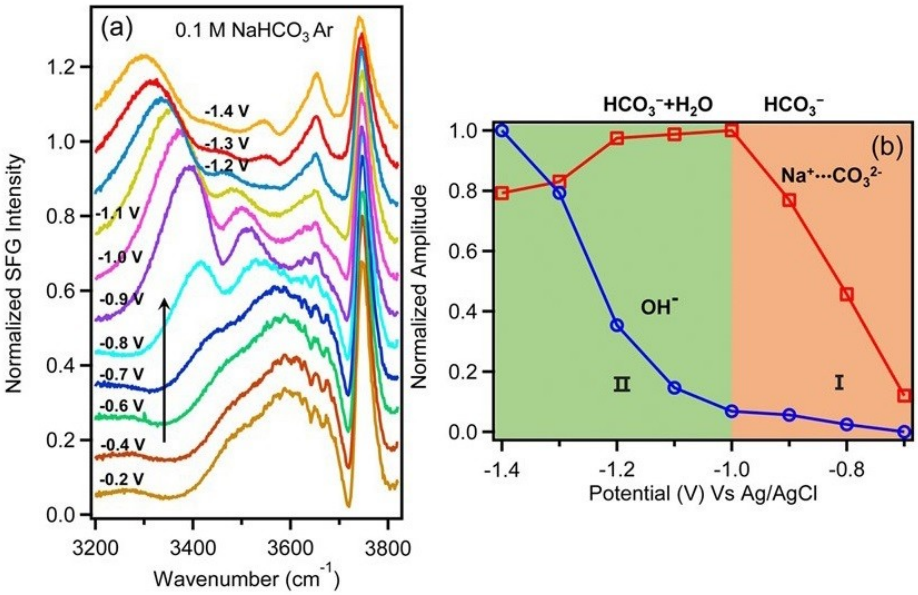

Figure 7. (a) VSFG spectra of water in Ar-purged 0.1 M $NaHCO_3$ solution as a function of applied potential. (b) Relative amplitudes of the carbonate feature (red curve) at around 3350 cm^{-1} and the OH^- feature (blue curve) at around 3650 cm^{-1} as a function of applied potential. Amplitudes of both peaks are independently normalized to their maximum intensity observed in the potential range between −0.2 to −1.4 V. Reprinted with permission from Ref. [67]. Copyright 2023 The Royal Society of Chemistry.

techniques, which would probe a few nm to a μm beyond the surface, where water molecules are already outside of the double layer.[74–77]

6. Future outlook on probing interfacial solvation structure during electrocatalysis

In this review, we have discussed application of plasmon-enhanced VSFG towards understanding the effect of cation composition and solvation at the electrode/electrolyte interface on electrocatalytic CO_2R. This technique enables monitoring reaction intermediates present at low coverage on a Au electrode during active electrocatalysis. The vibrational signatures of these intermediates serve as *in situ* probes of the Stern layer, carrying specific information of the electrode-electrolyte interfacial properties, such as local electric fields and cation-dependent solvation environment. These studies have shown that the solvation structure is site dependent as cations show different trends in the solvation radius at active compared to inactive sites. Additionally, the contribution of the solvation-induced Onsager reaction field may exceed the magnitude of the Stern layer electric field, and the catalytic reactivity is strongly correlated with the Onsager contribution of the electric field confirming the critical role that interfacial solvation structure plays on CO_2 activation. This technique also enables measurement of the potential dependent vibrational bands of interfacial water during both CO_2R and HER. From these measurements we can infer important information about the potential dependent proton source, where reduction of carbonate, bicarbonate, and water are in competition at the interface. Further interpretation of the water spectra to identify molecular motifs present in the double layer, such as ion-pairing and H-bond networks will require further support from theory. To address these questions, phase-dependent and heterodyne SFG could be helpful to obtain deeper insights into potential dependent water structure. Additionally, the $\chi^{(3)}$ effect on VSFG spectra also needs careful consideration, especially at high overpotential where the interfacial electric field is very strong and the $\chi^{(3)}$ contribution should not be neglected. In summary, this work lays the foundation for future experimental and theoretical studies, which will be important to understand how the molecular structure of interfacial solvation guides surface reaction kinetics in electrochemical systems. Based on the results described above, it is safe to conclude that treatment of interfacial solvation as a continuum dielectric is insufficient to provide a mechanistic understanding of specific ion effects and that molecular interactions involving both solvent molecules and specific cations play a significant role in the kinetics of CO_2 activation and reduction.

Acknowledgements

Development of the plasmon-enhanced VSFG method was supported by the National Science Foundation under NSF Award No. 1665280. Investigation of site-specific solvation structures, disentangling contributions to the interfacial electric field, and measurement of interfacial water spectra were supported by the Condensed Phase and Interfacial Molecular Science Program (CPIMS), in the Chemical Sciences Geosciences and Biosciences Division of the Office of Basic Energy Sciences of the U.S. Department of Energy under Contract No. DE-SC0020977.

Conflict of Interests

The authors declare no competing financial interest.

Data Availability Statement

Data sharing is not applicable to this article as no new data were created or analyzed in this study.

Keywords: electrochemistry · heterogenous catalysis · interfaces · solvent effects · vibrational spectroscopy

[1] A. D. Handoko, F. Wei, Jenndy, B. S. Yeo, Z. W. Seh, *Nature Catalysis* **2018**, *1*, 922.
[2] H. Mistry, Y.-W. Choi, A. Bagger, F. Scholten, C. S. Bonifacio, I. Sinev, N. J. Divins, I. Zegkinoglou, H. S. Jeon, K. Kisslinger, et al., *Angew. Chem.* **2017**, *129*, 11552.
[3] Y.-G. Kim, J. H. Baricuatro, A. Javier, J. M. Gregoire, M. P. Soriaga, *Langmuir* **2014**, *30*, 15053.
[4] R. G. Mariano, K. McKelvey, H. S. White, M. W. Kanan, *Science* **2017**, *358*, 1187.
[5] A. Eilert, F. Cavalca, F. S. Roberts, J. Osterwalder, C. Liu, M. Favaro, E. J. Crumlin, H. Ogasawara, D. Friebel, L. G. Pettersson, et al., *J. Phys. Chem. Lett.* **2017**, *8*, 285.
[6] F. Calle-Vallejo, M. T. Koper, *Angew. Chem.* **2013**, *125*, 7423.
[7] G. Marcandalli, A. Goyal, M. T. Koper, *ACS Catal.* **2021**, *11*, 4936.
[8] E. Pérez-Gallent, M. C. Figueiredo, F. Calle-Vallejo, M. T. Koper, *Angew. Chem. Int. Ed.* **2017**, *56*, 3621.
[9] J. Li, X. Li, C. M. Gunathunge, M. M. Waegele, *Proc. Natl. Acad. Sci. USA* **2019**, *116*, 9220.
[10] C. M. Gunathunge, J. Li, X. Li, J. J. Hong, M. M. Waegele, *ACS Catal.* **2020**, *10*, 6908.
[11] C. M. Gunathunge, J. Li, X. Li, M. M. Waegele, *ACS Catal.* **2020**, *10*, 11700.
[12] S. Sarkar, A. Maitra, S. Banerjee, V. S. Thoi, J. M. Dawlaty, *J. Phys. Chem. B* **2020**, *124*, 1311.
[13] D. Bhattacharyya, P. E. Videla, M. Cattaneo, V. S. Batista, T. Lian, C. P. Kubiak, *Chem. Sci.* **2021**, *12*, 10131.
[14] M. R. Singh, Y. Kwon, Y. Lum, J. W. Ager III, A. T. Bell, *J. Am. Chem. Soc.* **2016**, *138*, 13006.
[15] Q. Zhu, S. K. Wallentine, G.-H. Deng, J. A. Rebstock, L. R. Baker, *JACS Au* **2022**, *2*, 472.
[16] A. Frumkin, *Trans. Faraday Soc.* **1959**, *55*, 156.
[17] Y. Hori, S. Suzuki, *Bull. Chem. Soc. Jpn.* **1982**, *55*, 660.
[18] J. Resasco, L. D. Chen, E. Clark, C. Tsai, C. Hahn, T. F. Jaramillo, K. Chan, A. T. Bell, *J. Am. Chem. Soc.* **2017**, *139*, 11277.
[19] L. D. Chen, M. Urushihara, K. Chan, J. K. Nørskov, *ACS Catal.* **2016**, *6*, 7133.
[20] M. C. Monteiro, F. Dattila, B. Hagedoorn, R. García-Muelas, N. López, M. T. Koper, *Nature Catalysis* **2021**, *4*, 654.
[21] S. Mezzavilla, S. Horch, I. E. Stephens, B. Seger, I. Chorkendorff, *Angew. Chem. Int. Ed.* **2019**, *58*, 3774.
[22] G. Marcandalli, M. Villalba, M. T. Koper, *Langmuir* **2021**, *37*, 5707.
[23] S. Back, M. S. Yeom, Y. Jung, *ACS Catal.* **2015**, *5*, 5089.
[24] S. Wallentine, S. Bandaranayake, S. Biswas, L. R. Baker, *J. Phys. Chem. A* **2020**, *124*, 8057.
[25] J. A. Rebstock, Q. Zhu, L. R. Baker, *Chem. Sci.* **2022**, *13*, 7634.

[26] S. Wallentine, S. Bandaranayake, S. Biswas, L. R. Baker, *J. Phys. Chem. Lett.* **2020**, *11*, 8307.
[27] A. Lagutchev, S. A. Hambir, D. D. Dlott, *J. Phys. Chem. C* **2007**, *111*, 13645.
[28] A. Lagutchev, A. Lozano, P. Mukherjee, S. A. Hambir, D. D. Dlott, *Spectrochim. Acta Part A* **2010**, *75*, 1289.
[29] A. D. Curtis, S. B. Reynolds, A. R. Calchera, J. E. Patterson, *J. Phys. Chem. Lett.* **2010**, *1*, 2435.
[30] E. H. Backus, N. Garcia-Araez, M. Bonn, H. J. Bakker, *J. Phys. Chem. C* **2012**, *116*, 23351.
[31] A. Wuttig, Y. Surendranath, *ACS Catal.* **2015**, *5*, 4479.
[32] Y. Hori, H. Konishi, T. Futamura, A. Murata, O. Koga, H. Sakurai, K. Oguma, *Electrochim. Acta* **2005**, *50*, 5354.
[33] C. H. Bartholomew, *Appl. Catal. A* **2001**, *212*, 17.
[34] S. Ringe, E. L. Clark, J. Resasco, A. Walton, B. Seger, A. T. Bell, K. Chan, *Energy Environ. Sci.* **2019**, *12*, 3001.
[35] G. Hussain, L. Pérez-Martínez, J.-B. Le, M. Papasizza, G. Cabello, J. Cheng, A. Cuesta, *Electrochim. Acta* **2019**, *327*, 135055.
[36] M. Liu, Y. Pang, B. Zhang, P. De Luna, O. Voznyy, J. Xu, X. Zheng, C. T. Dinh, F. Fan, C. Cao, et al., *Nature* **2016**, *537*, 382.
[37] S.-G. Sun, W.-B. Cai, L.-J. Wan, M. Osawa, *J. Phys. Chem. B* **1999**, *103*, 2460.
[38] J. A. Rodriguez, C. M. Truong, D. W. Goodman, *J. Chem. Phys.* **1992**, *96*, 7814.
[39] G. Bistoni, S. Rampino, N. Scafuri, G. Ciancaleoni, D. Zuccaccia, L. Belpassi, F. Tarantelli, *Chem. Sci.* **2016**, *7*, 1174.
[40] W.-L. Yim, T. Nowitzki, M. Necke, H. Schnars, P. Nickut, J. Biener, M. M. Biener, V. Zielasek, K. Al-Shamery, T. Klüner, et al., *J. Phys. Chem. C* **2007**, *111*, 445.
[41] X. Chang, H. Xiong, Y. Xu, Y. Zhao, Q. Lu, B. Xu, *Catalysis Science, Technology* **2021**, *11*, 6825.
[42] Y. Liu, T. Kawaguchi, M. S. Pierce, V. Komanicky, H. You, *J. Phys. Chem. Lett.* **2018**, *9*, 1265.
[43] P. Suppan, *J. Photochem. Photobiol. A* **1990**, *50*, 293.
[44] C. J. Reckmeier, Y. Wang, R. Zboril, A. L. Rogach, *J. Phys. Chem. C* **2016**, *120*, 10591.
[45] J. K. Denton, P. J. Kelleher, M. A. Johnson, M. D. Baer, S. M. Kathmann, C. J. Mundy, B. A. Wellen Rudd, H. C. Allen, T. H. Choi, K. D. Jordan, *Proc. Natl. Acad. Sci. USA* **2019**, *116*, 14874.
[46] J.-H. Choi, M. Cho, *J. Chem. Phys.* **2011**, *134*, 154513.
[47] S. A. Sorenson, J. G. Patrow, J. M. Dawlaty, *J. Am. Chem. Soc.* **2017**, *139*, 2369.
[48] N. M. Levinson, S. D. Fried, S. G. Boxer, *J. Phys. Chem. B* **2012**, *116*, 10470.
[49] I. T. Suydam, C. D. Snow, V. S. Pande, S. G. Boxer, *Science* **2006**, *313*, 200.
[50] S. D. Fried, S. Bagchi, S. G. Boxer, *Science* **2014**, *346*, 1510.
[51] M. L. Clark, A. Ge, P. E. Videla, B. Rudshteyn, C. J. Miller, J. Song, V. S. Batista, T. Lian, C. P. Kubiak, *J. Am. Chem. Soc.* **2018**, *140*, 17643.
[52] A. Jafarzadeh, K. M. Bal, A. Bogaerts, E. C. Neyts, *J. Phys. Chem. C* **2020**, *124*, 6747.
[53] I. V. Chernyshova, S. Ponnurangam, *Phys. Chem. Chem. Phys.* **2019**, *21*, 8797.
[54] J. Kim, P. S. Cremer, *J. Am. Chem. Soc.* **2000**, *122*, 12371.
[55] C. Tian, Y. Shen, *Proc. Natl. Acad. Sci. USA* **2009**, *106*, 15148.
[56] E. H. Backus, J. Schaefer, M. Bonn, *Angew. Chem. Int. Ed.* **2021**, *60*, 10482.
[57] B. Rehl, E. Ma, S. Parshotam, E. L. DeWalt-Kerian, T. Liu, F. M. Geiger, J. M. Gibbs, *J. Am. Chem. Soc.* **2022**, *144*, 16338.
[58] S. M. Piontek, M. DelloStritto, B. Mandal, T. Marshall, M. L. Klein, E. Borguet, *J. Am. Chem. Soc.* **2020**, *142*, 12096.
[59] G.-H. Deng, Y. Shen, H. Chen, Y. Chen, B. Jiang, G. Wu, X. Yang, K. Yuan, J. Zheng, *J. Phys. Chem. Lett.* **2019**, *10*, 7922.
[60] S. Strazdaite, J. Versluis, H. J. Bakker, *J. Chem. Phys.* **2015**, *143*.
[61] E. A. Raymond, T. L. Tarbuck, M. G. Brown, G. L. Richmond, *J. Phys. Chem. B* **2003**, *107*, 546.
[62] W. Gan, D. Wu, Z. Zhang, R.-r. Feng, H.-f. Wang, *J. Chem. Phys.* **2006**, *124*, 114705.
[63] S. Nihonyanagi, S. Yamaguchi, T. Tahara, *J. Am. Chem. Soc.* **2010**, *132*, 6867.
[64] G.-H. Deng, X. Li, S. Liu, Z. Zhang, Z. Lu, Y. Guo, *J. Phys. Chem. C* **2016**, *120*, 12032.
[65] D. Liu, G. Ma, L. M. Levering, H. C. Allen, *J. Phys. Chem. B* **2004**, *108*, 2252.
[66] Y. Tong, F. Lapointe, M. Thämer, M. Wolf, R. K. Campen, *Angew. Chem. Int. Ed.* **2017**, *56*, 4211.
[67] G.-H. Deng, Q. Zhu, J. Rebstock, T. Neves-Garcia, L. R. Baker, *Chem. Sci.* **2023**, *14*, 4523.
[68] Y. R. Shen, V. Ostroverkhov, *Chem. Rev.* **2006**, *106*, 1140.
[69] A. Eftekhari-Bafrooei, E. Borguet, *J. Phys. Chem. Lett.* **2011**, *2*, 1353.
[70] P. Li, Y. Jiang, Y. Hu, Y. Men, Y. Liu, W. Cai, S. Chen, *Nature Catalysis* **2022**, *5*, 900.
[71] M. M. Waegele, C. M. Gunathunge, J. Li, X. Li, *J. Chem. Phys.* **2019**, *151*, 160902.
[72] W. Deng, T. Yuan, S. Chen, H. Li, C. Hu, H. Dong, B. Wu, T. Wang, J. Li, G. A. Ozin, et al., *Fundam. Res* **2021**, *1*, 432.
[73] M. Dunwell, X. Yang, B. P. Setzler, J. Anibal, Y. Yan, B. Xu, *ACS Catal.* **2018**, *8*, 3999.
[74] A. Götz, R. Nikzad-Langerodi, Y. Staedler, A. Bellaire, J. Saukel, *Spectrochim. Acta Part A* **2020**, *224*, 117460.
[75] W. S. Yoo, B. G. Kim, S. W. Jin, T. Ishigaki, K. Kang, *ECS J. Solid State Sci. Technol.* **2014**, *3*, N142.
[76] G. Kumari, J. Kandula, C. Narayana, *J. Phys. Chem. C* **2015**, *119*, 20057.
[77] K. Ataka, S. T. Stripp, J. Heberle, *Biochim. Biophys. Acta BBA-Biomembr.* **2013**, *1828*, 2283.

Manuscript received: October 18, 2023
Revised manuscript received: January 5, 2024
Accepted manuscript online: January 10, 2024
Version of record online: February 6, 2024